
DYNAMIC PROBABILISTIC PREDICTABLE FEATURE ANALYSIS FOR MULTIVARIATE TEMPORAL PROCESS MONITORING

A PREPRINT

 **Wei Fan**

Key Laboratory of Energy Thermal Conversion
and Control of Ministry of Education
Southeast University
Nanjing 210096, China
wfan@seu.edu.cn

Qinqin Zhu*

Department of Chemical Engineering
University of Waterloo
ON N2L 3G1, Canada
qinqin.zhu@uwaterloo.ca

Shaojun Ren*

Key Laboratory of Energy Thermal
Conversion and Control of Ministry of Education
Southeast University
Nanjing 210096, China
rsj@seu.edu.cn

Liang Zhang

School of Instrument Science and Engineering
Key Laboratory of Micro-Inertial Instrument
and Advanced Navigation Technology
of Ministry of Education
Southeast University
Nanjing 210096, China
zhangliang418@seu.edu.cn

Fengqi Si

Key Laboratory of Energy Thermal Conversion
and Control of Ministry of Education
Southeast University
Nanjing 210096, China
fqsi@seu.edu.cn

March 2, 2022

ABSTRACT

Dynamic statistical process monitoring methods have been widely studied and applied in modern industrial processes. These methods aim to extract the most predictable temporal information and develop the corresponding dynamic monitoring schemes. However, measurement noise is widespread in real-world industrial processes, and ignoring its effect will lead to sub-optimal modeling and monitoring performance. In this article, a probabilistic predictable feature analysis (PPFA) is proposed for multivariate time series modeling, and a multi-step dynamic predictive monitoring scheme is developed. The model parameters are estimated with an efficient expectation-maximum algorithm, where the genetic algorithm and Kalman filter are designed and incorporated. Further, a novel dynamic statistical monitoring index, Dynamic Index, is proposed as an important supplement of T^2 and SPE to detect dynamic anomalies. The effectiveness of the proposed algorithm is demonstrated via its application on the three-phase flow facility and a medium speed coal mill.

Keywords Dynamic process monitoring, probabilistic predictable feature analysis, EM algorithm, genetic algorithm, Kalman filter.

*co-corresponding authors, equal contribution

1 Introduction

In the current era of big data, industrial processes are equipped with a large number of sensors to measure different process variables. At the same time, massive amounts of historical data are collected and stored. On this basis, data-driven process monitoring has become a popular research topic due to its reliable performance and easy-to-implement characteristics [Severson et al., 2016, Ge, 2017, Zhou et al., 2016]. Multivariate statistical process monitoring method is a representative kind, including principal component analysis (PCA) [Alcala and Qin, 2009], partial least squares [Li et al., 2010] and canonical component analysis [Zhu et al., 2017]. As a dimensionality reduction algorithm, PCA decomposes the measurement space into principal component subspace and residual subspace, and realizes industrial process monitoring by designing relevant statistical indices. However, traditional PCA does not take temporal information into account, and thus tends to obtain sub-optimal performance.

To tackle the inevitable dynamics in the data samples, several extensions have been proposed. Ku et al. [Ku et al., 1995] proposed a dynamic PCA (DPCA), which employs augmented measurements with time lags and tries to explore the serial correlations between current and previous observations. With the derived relations, statistical indices such as T^2 and SPE are employed to monitor abnormal condition of industrial processes. Rato and Reis [Rato and Reis, 2013] and Vanhatalo et al. [Vanhatalo et al., 2017] further improved DPCA in auto-correlation extraction and the selection of time lags respectively. Though some dynamics are exploited by these models, their internal structure is still static. Besides, DPCA fails to provide an explicit expression between latent variables and observed measurements, and the interpretability of the established model is limited [Dong and Qin, 2018].

To address the aforementioned issues, Li et al. [Li et al., 2014] proposed the vector auto-regressive (VAR) model, in which the concept of inner model was put forward. This method gives an explicit expression of the dynamic relation of latent variables, but its inner model is not consistent with the outer model, leading to sub-optimal monitoring performance [Guo et al., 2020]. Motivated by the concept of VAR, Dong and Qin [Dong and Qin, 2018] designed VAR in both inner and outer models, and developed a novel dynamic inner PCA (DiPCA) method to capture the most dynamic variations from time series data. Similarly, Richthofer and Wiskott [Richthofer and Wiskott, 2015] proposed the predictable feature analysis (PFA) to extract dynamic latent variables that are as predictable as possible. Both DiPCA and PFA are efficient auto-regressive models, and their difference lies in the design of their objective functions. DiPCA builds a model by maximizing the covariance between the actual value and estimated value of the latent variable, while PFA aims to minimize the auto-regressive prediction error of the latent variable.

In practical engineering applications, the variables are inevitable to be polluted by random noise, which, however, are not considered in the aforementioned methods. To provide the complete distribution of the data, the dynamic characteristics of process variables should be extracted through statistical patterns rather than deterministic manner [Zheng et al., 2016]. Based on the above analysis, this article is dedicated to exploring the integration of probabilistic models and traditional VAR-based methods, and applying them for dynamic predictive process monitoring. Inspired by the state space expressions designed in probabilistic PCA (PPCA) [Tipping and Bishop, 1999] and probabilistic slow feature analysis (PSFA) [Guo et al., 2016], we extend DiPCA and PFA to a probabilistic structure, referred to as probabilistic predictable feature analysis (PPFA). A high-order linear Markov state-space form is designed in PPFA to represent the weighted relations among its latent variables, and thus to model their dynamics. It is worthwhile to point out that PPFA has intrinsic advantages over DiPCA and PFA. First, deterministic methods fail to grasp the distribution of measurement noise, while PPFA overcomes this problem with a fully probabilistic framework. On the other hand, inspired by the nonstationary PSFA [Scott et al., 2020], a monitoring statistic, Dynamic Index (DI), is derived to demonstrate the dynamic changes of studied systems, thereby providing a reliable guidance for improving control performance. The Expectation-Maximization (EM) algorithm [Dempster et al., 1977] and Kalman filter [Bishop, 2006] are adopted to estimate the model parameters of PPFA. The main contributions of this work are

- A novel probabilistic extension of DiPCA and PFA, termed as PPFA, is designed, which provides a full interpretation of the dynamic characteristics of both measurements and latent variables.
- Multiple time lags are designed in PPFA to capture the actual dynamics involved in the data.
- In M-step of the EM algorithm, the genetic algorithm (GA) [Goldberg and Holland, 1988] is employed to optimize the weight coefficients of latent variables, which are difficult to be solved analytically.
- During the procedure of E-step, an expansion method of latent structure is proposed to estimate relevant expectations of the high-order dynamic system with Kalman filter.
- Based on the proposed PPFA model, three monitoring statistics, T^2 , SPE and DI, are developed for process monitoring.

The rest of this paper is organized as follows. Section 2 presents a brief introduction of DiPCA and PFA. In Section 3, the detailed derivation of PPFA as well as the novel PPFA-based dynamic process monitoring framework are

demonstrated. Then, experiments on the three-phase flow facility and a medium speed coal mill are presented to testify the effectiveness of the proposed PPFA-based modeling and monitoring method. Finally, conclusions are drawn in Section 5.

2 Preliminary

2.1 Dynamic inner Principal Component Analysis

DiPCA is a dynamic extension of PCA that exploits temporal information from the data space to form its dynamic latent variables [Dong and Qin, 2018]. DiPCA aims to predict the current score with the past s samples. Mathematically, it is expressed as

$$t_k = \sum_{j=1}^s \beta_j t_{k-j} + e_k \quad (1)$$

where $t_k = \mathbf{x}_k^\top \mathbf{w}$ is the latent score for the observed sample \mathbf{x}_k at time k , \mathbf{w} is the weight vector, e_k is the modeling error, s is the time lag, and β_j is the auto-regressive coefficient. It is assumed that e_k is white noise if s is long enough, such that the estimated prediction of latent variable is expressed as

$$\begin{aligned} \hat{t}_k &= \mathbf{x}_{k-1}^\top \mathbf{w} \beta_1 + \cdots + \mathbf{x}_{k-s}^\top \mathbf{w} \beta_s \\ &= [\mathbf{x}_{k-1}^\top \cdots \mathbf{x}_{k-s}^\top] (\boldsymbol{\beta} \otimes \mathbf{w}) \end{aligned} \quad (2)$$

where $\boldsymbol{\beta} = [\beta_1, \beta_2, \cdots, \beta_s]^\top$, and $\boldsymbol{\beta} \otimes \mathbf{w}$ is the Kronecker product.

Denote the data matrix as $\mathbf{X} = [\mathbf{x}_1^\top, \mathbf{x}_2^\top, \cdots, \mathbf{x}_{n+s}^\top]^\top \in \mathbb{R}^{(n+s) \times m}$, and define a new data matrix containing temporal information $\mathbf{Z}_s = [\mathbf{X}_1, \mathbf{X}_2, \cdots, \mathbf{X}_s]$, where $\mathbf{X}_j = [\mathbf{x}_j^\top, \mathbf{x}_{j+1}^\top, \cdots, \mathbf{x}_{n+j-1}^\top]^\top$, $j = 1, 2, \cdots, s$. Then the objective of DiPCA in Eq. (1) can be represented as the following matrix form.

$$\begin{aligned} \max_{\mathbf{w}, \boldsymbol{\beta}} \quad & \mathbf{w}^\top \mathbf{X}_{s+1}^\top \mathbf{Z}_s (\boldsymbol{\beta} \otimes \mathbf{w}) \\ \text{s.t.} \quad & \|\mathbf{w}\| = 1, \quad \|\boldsymbol{\beta}\| = 1 \end{aligned} \quad (3)$$

More details of extracting dynamic components for DiPCA can be found in ref. [Dong and Qin, 2018].

2.2 Predictable Feature Analysis

Similar to DiPCA, PFA is also an auto-regressive model, and it focuses on measuring the predictability of the extracted latent variables [Richthofer and Wiskott, 2015]. PFA defines that a good predictability is achieved when the latent score can be well predicted by a linear combination of s past values. Given an m -dimensional temporal measurement \mathbf{x}_k , PFA aims to find an orthogonal transformation $\mathbf{W} \in \mathbb{R}^{m \times r}$, such that the projection $\mathbf{t}_k = \mathbf{x}_k^\top \mathbf{W}$ obtains the highest predictability. Mathematically, given the coefficient matrices $\mathbf{B}_i \in \mathbb{R}^{r \times r}$, $1 \leq i \leq s$, the prediction of \mathbf{t}_k is

$$\hat{\mathbf{t}}_k = \sum_{i=j}^s \mathbf{B}_j \mathbf{t}_{k-j} = \sum_{j=1}^s \mathbf{B}_j \mathbf{W}^\top \mathbf{x}_{k-j} \quad (4)$$

where the modeling error is omitted. It is observed that both Eq. (1) and Eq. (4) share similar structure, and both of them aim to extract the most predictable latent variables. Their main difference is that the goal of DiPCA is to maximize the covariance between t_k and \hat{t}_k , while PFA solves the auto-regressive issue by minimizing the prediction error, which is expressed as

$$\min_{\mathbf{W}} \left\langle \left\| \mathbf{W}^\top \mathbf{x}_k - \sum_{j=1}^s \mathbf{B}_j \mathbf{W}^\top \mathbf{x}_{k-j} \right\|^2 \right\rangle \quad (5)$$

where $\langle \cdot \rangle$ means the average of signals over time. Readers can refer to ref. [Richthofer and Wiskott, 2015] for the detailed PFA algorithm.

3 Methodology

3.1 Probabilistic Predictable Feature Analysis

In real-world industrial processes, the variables are inevitable to be polluted by random noise, which are not considered in both DiPCA and PFA. To improve the prediction performance, the dynamic characteristics of process variables

should be extracted through statistical patterns rather than deterministic manner [Zheng et al., 2016]. Therefore, this work is to extend DiPCA and PFA to a probabilistic structure with a state-space form, referred to as probabilistic predictable feature analysis (PPFA), which describes the process dynamics in a more compact and clearer manner.

Given the collected samples $\mathbf{X} = [\mathbf{x}_1^\top \mathbf{x}_2^\top \cdots \mathbf{x}_{n+s}^\top]^\top$, PPFA takes the following generative state-space form

$$\begin{cases} \mathbf{t}_k = \sum_{j=1}^s \mathbf{B}_j \mathbf{t}_{k-j} + \mathbf{e}_k \\ \mathbf{x}_k = \mathbf{H} \mathbf{t}_k + \boldsymbol{\varepsilon}_k \end{cases} \quad (6)$$

s.t. $\mathbb{E}[\mathbf{t}_k] = \mathbf{0}$, $\mathbb{E}[\mathbf{t}_k \mathbf{t}_k^\top] = \mathbf{I}_r$

where $\mathbf{H} \in \mathbb{R}^{m \times r}$ represents the emission matrix, $\mathbf{B}_j = \text{diag}\{\beta_j^1, \dots, \beta_j^r\}$, ($1 \leq j \leq s$) denotes the transition matrix, $\mathbf{e}_k \sim \mathcal{N}(\mathbf{0}, \boldsymbol{\Gamma})$ with $\boldsymbol{\Gamma} = \text{diag}\{\tau_1^2, \dots, \tau_r^2\}$ is the Gaussian distributed noise, $\boldsymbol{\varepsilon}_k \sim \mathcal{N}(\mathbf{0}, \boldsymbol{\Sigma})$ with $\boldsymbol{\Sigma} = \text{diag}\{\sigma_1^2, \dots, \sigma_m^2\}$ is the measurement noise, and \mathbf{I}_r is an $r \times r$ identity matrix.

Lemma 1 Given the constraints in Eq. (6) that $\mathbb{E}(\mathbf{t}_k) = \mathbf{0}$ and $\mathbb{E}(\mathbf{t}_k \mathbf{t}_k^\top) = \mathbf{I}_r$, the relation between \mathbf{B}_j and $\boldsymbol{\Gamma}$ is

$$\tau_i^2 = 1 - \sum_{j=1}^s \beta_j^i \gamma_j^i \geq 0, \quad 1 \leq i \leq r \quad (7)$$

where $\gamma_j^i = \text{cov}(t_k^i, t_{k-j}^i) = \text{cov}(t_{k+j}^i, t_k^i)$ is the autocovariance, and t_k^i with $1 \leq i \leq r$ represents the i^{th} latent variable at time k .

The proof of Lemma 1 is given in APPENDIX A, and the expression of γ_j^i is also provided in the appendix. For PPFA, the parameters needed to be estimated are summarized as $\boldsymbol{\Theta} = \{\mathbf{B}_j \ (1 \leq j \leq s), \mathbf{H}, \boldsymbol{\Gamma}, \boldsymbol{\Sigma}\}$.

The maximum-likelihood method is widely used for parameter optimization of probabilistic models. Given the temporal series \mathbf{X} , the complete data log-likelihood of the dynamic system in Eq. (6) can be given by

$$\begin{aligned} L(\boldsymbol{\Theta}) &= \log p(\mathbf{X}, \mathbf{T} | \boldsymbol{\Theta}) \\ &= \log \prod_{k=s+1}^{n+s} \left[p(\mathbf{t}_k | \{\mathbf{t}_{k-j}\}_{j=1}^s) p(\mathbf{x}_k | \mathbf{t}_k) \right] \\ &\quad \times \prod_{k=1}^s [p(\mathbf{t}_k) p(\mathbf{x}_k | \mathbf{t}_k)] \\ &= \sum_{k=1}^s \log p(\mathbf{t}_k) + \sum_{k=1}^{n+s} \log p(\mathbf{x}_k | \mathbf{t}_k) \\ &\quad + \sum_{k=s+1}^{n+s} p(\mathbf{t}_k | \{\mathbf{t}_{k-j}\}_{j=1}^s) \end{aligned} \quad (8)$$

where $\mathbf{T} = [\mathbf{t}_1^\top, \mathbf{t}_2^\top, \dots, \mathbf{t}_{s+n}^\top]^\top \in \mathbb{R}^{(n+s) \times r}$ denotes the latent variables matrix.

For each sample \mathbf{x}_k , based on the property of conditional independence, the corresponding high-order linear Markov Gaussian dynamic system $p(\mathbf{t}_k | \{\mathbf{t}_{k-j}\}_{j=1}^s)$ in Eq. (8) is expressed as

$$\begin{aligned} p(\mathbf{t}_k | \{\mathbf{t}_{k-j}\}_{j=1}^s) &\equiv p(\mathbf{t}_k | \{\mathbf{t}_{k-j}\}_{j=1}^s, \{\mathbf{B}_j\}_{j=1}^s, \boldsymbol{\Gamma}) \\ &= \prod_{i=1}^r p(t_k^i | \{t_{k-j}^i\}_{j=1}^s, \{\beta_j^i\}_{j=1}^s, \tau_i^2) \end{aligned} \quad (9)$$

where

$$p(t_k^i | \{t_{k-j}^i\}_{j=1}^s, \{\beta_j^i\}_{j=1}^s, \tau_i^2) = \mathcal{N}\left(\sum_{j=1}^s \beta_j^i t_{k-j}^i, \tau_i^2\right) \quad (10)$$

$$p(\mathbf{t}_1) = p(\mathbf{t}_2) = \cdots = p(\mathbf{t}_s) = \mathcal{N}(\mathbf{0}, \mathbf{I}_r) \quad (11)$$

The probabilistic distribution of the mapping from \mathbf{t}_k to \mathbf{x}_k in Eq. (8) is

$$p(\mathbf{x}_k | \mathbf{t}_k) \equiv p(\mathbf{x}_k | \mathbf{t}_k, \mathbf{H}, \Sigma) = \mathcal{N}(\mathbf{H}\mathbf{t}_k, \Sigma) \quad (12)$$

The complete specification of PPFA is defined in Eqs. (8) to (12), and the parameter set Θ can be obtained via maximizing $L(\Theta)$ in Eq. (8). It is noted that both stochastic design and multi-step time lags are considered in PPFA in Eq. (6), and several challenging issues should be addressed. Firstly, much more parameters in Θ need to be determined, and a more efficient EM method should be designed. Further, the analytical solutions cannot be derived for β_j^i in \mathbf{B}_j , and an optimization method should be integrated with the EM method. Additionally, for the high-order state-space model in Eq. (6), the expectations of the latent variables cannot be directly estimated with the traditional Kalman smoothing method [Bishop, 2006]. In the following subsections, the traditional EM algorithm and Kalman smoothing method is optimized to address the aforementioned issues.

3.2 Parameter Estimation Scheme

The EM algorithm is a powerful method to solve the parameter estimation problem of probabilistic generative models through two steps of continuous iteration, namely E-step and M-step. In this section, we give detailed derivation process of EM algorithm applied in PPFA. The main body of parameter estimation process is the EM algorithm; however, it is difficult to obtain explicit analytical solutions for parameters β_j^i . Thus, GA algorithm is embedded into the EM process to construct the complete parameter optimization strategy.

3.2.1 EM Algorithm

Substituting the probability density function in Eqs. (9)-(12) into Eq. (8), we have

$$\begin{aligned} L(\Theta) = & -\frac{(n+s)(r+m)}{2} \log(2\pi) - \frac{1}{2} \sum_{k=1}^s (\mathbf{t}_k^\top \mathbf{t}_k) \\ & - n \sum_{i=1}^r \log(\tau_i) - \frac{1}{2} \sum_{k=1}^{n+s} [(\mathbf{x}_k - \mathbf{H}\mathbf{t}_k)^\top \Sigma^{-1} (\mathbf{x}_k - \mathbf{H}\mathbf{t}_k)] \\ & - \frac{(n+s)}{2} \log|\Sigma| - \frac{1}{2} \sum_{k=s+1}^{n+s} \sum_{i=1}^r \frac{1}{\tau_i^2} \left[\tau_k^i - \sum_{j=1}^s \beta_j^i t_{k-j}^i \right] \end{aligned}$$

The Q -function is defined conditioned on the old parameter set Θ^{old} as

$$Q(\Theta, \Theta^{\text{old}}) = \mathbb{E}_{\mathbf{X}, \Theta^{\text{old}}} \{L(\Theta)\} \quad (13)$$

Then, in the M-step, new parameters are estimated through

$$\Theta^{\text{new}} = \arg \max_{\Theta} Q(\Theta, \Theta^{\text{old}}) \quad (14)$$

Since \mathbf{B}_j ($1 \leq j \leq s$) and Γ are related to each other as shown in *Lemma 1*, the parameter set to be estimated can be simplified to $\Theta = \{\mathbf{B}_j, 1 \leq j \leq s, \mathbf{H}, \Sigma\}$. Then take derivatives of Q -function with respect to different parameters in Θ . First of all, for β_j^i in \mathbf{B}_j , taking the derivation leads to

$$\frac{\partial Q(\Theta, \Theta^{\text{old}})}{\partial \beta_j^i} = \frac{n\gamma_j^i}{2(1 - \sum_{l=1}^s \beta_l^i \gamma_l^i)} - \frac{1}{2} \sum_{k=s+1}^{n+s} \frac{\gamma_j^i [t_k^i - \sum_{l=1}^s \beta_l^i t_{k-l}^i]^2}{1 - \sum_{l=1}^s \beta_l^i \gamma_l^i} - \frac{1}{2} \sum_{k=s+1}^{n+s} 2t_{k-j}^i \left[t_k^i - \sum_{l=1}^s \beta_l^i t_{k-l}^i \right] = 0$$

Then setting the above equation to zero, we have

$$\begin{aligned} & \left[n\gamma_j^i - 2 \sum_{l=1}^s \beta_l^i \sum_{k=s+1}^{n+s} t_{k-j}^i t_{k-l}^i + 2 \sum_{k=s+1}^{n+s} t_k^i t_{k-j}^i \right] \\ & \times \left(1 - \sum_{l=1}^s \beta_l^i \gamma_l^i \right) = 2 \sum_{l=1}^s \sum_{g=l+1}^s \beta_l^i \beta_g^i \times \sum_{k=s+1}^{n+s} (t_{k-j}^i t_{k-g}^i) \\ & + \gamma_j^i \left[\sum_{k=s+1}^{n+s} (t_k^i)^2 - 2 \sum_{l=1}^s \beta_l^i \sum_{k=s+1}^{n+s} t_k^i t_{k-l}^i + \sum_{l=1}^s (\beta_l^i)^2 \sum_{k=s+1}^{n+s} (t_{k-l}^i)^2 \right] \end{aligned} \quad (15)$$

It is difficult to derive the analytical solution for Eq. (15). Alternatively, GA algorithm is employed to simplify the derivation, which is demonstrated in the next subsection.

For parameter matrix \mathbf{H} , differentiating $Q(\Theta, \Theta^{\text{old}})$ with respect to it and setting it to zero result in

$$\mathbf{H}^{\text{new}} = \left(\sum_{k=1}^{n+s} \mathbf{x}_k \mathbf{t}_k^\top \right) \left(\sum_{k=1}^{n+s} \mathbf{t}_k \mathbf{t}_k^\top \right)^{-1} \quad (16)$$

Similarly, the covariance parameter Σ is updated with

$$\Sigma^{\text{new}} = \frac{1}{n+s} \sum_{k=1}^{n+s} (\mathbf{x}_k - \mathbf{H}^{\text{new}} \mathbf{t}_k) (\mathbf{x}_k - \mathbf{H}^{\text{new}} \mathbf{t}_k)^\top \quad (17)$$

It is noted that $\Sigma = \text{diag} \{ \sigma_1^2, \dots, \sigma_m^2 \}$, and each σ_i^2 in Σ can be calculated by

$$\sigma_i^2 = \frac{1}{n+s} \sum_{k=1}^{n+s} \left\{ (x_k^i)^2 - 2\mathbf{h}_i^\top \mathbf{t}_k x_k^i + \mathbf{h}_i^\top \mathbf{t}_k \mathbf{t}_k^\top \mathbf{h}_i \right\} \quad (18)$$

where $\mathbf{h}_i = [h_i^1, \dots, h_i^r]^\top$ is the i^{th} row of \mathbf{H}^{new} .

During the process of M-step, the following expectations with respect to the latent variables \mathbf{t}_k should be evaluated, which will be further utilized in the E-step given the old parameter set Θ^{old} .

$$\begin{aligned} & \mathbb{E}_{\mathbf{t}_k | \mathbf{x}_k, \Theta^{\text{old}}} [\mathbf{t}_k] \\ & \mathbb{E}_{\mathbf{t}_k | \mathbf{x}_k, \Theta^{\text{old}}} [\mathbf{t}_k \mathbf{t}_k^\top] \\ & \mathbb{E}_{\mathbf{t}_k | \mathbf{x}_k, \Theta^{\text{old}}} [\mathbf{t}_k \mathbf{t}_{k-l}^\top], 1 \leq l \leq s \\ & \mathbb{E}_{\mathbf{t}_k | \mathbf{x}_k, \Theta^{\text{old}}} [\mathbf{t}_{k-l} \mathbf{t}_{k-g}^\top], 1 \leq l, g \leq s \end{aligned} \quad (19)$$

Eq. (19) will be further investigated in Subsection "Expectation Estimation Strategy".

3.2.2 Genetic Algorithm

The genetic algorithm is adopted to get the values of β_j^i in Eq. (15). GA is an adaptive heuristic optimization algorithm proposed on the basis of natural selection in the theory of evolution [Goldberg and Holland, 1988]. The main idea of GA is to model the system that satisfies the natural evolution conditions, and solve the optimization problem by randomly searching the pre-constructed search space. During the iterative process, the population is mutated and reorganized, and the fitness function is used to evaluate the reliability of individuals. In the end, individuals who adapt to the system environment are evolved, and the best one is selected as the parameter candidate [Garg, 2016].

To estimate β_j^i , the optimization model is constructed as follows. Based on Eq. (15), two reference indices A and B are defined as follows

$$\begin{aligned} \text{A} = & \left[n\gamma_j^i - 2 \sum_{l=1}^s \beta_l^i \sum_{k=s+1}^{n+s} t_{k-j}^i t_{k-l}^i + 2 \sum_{k=s+1}^{n+s} t_k^i t_{k-j}^i \right] \\ & \times \left(1 - \sum_{l=1}^s \beta_l^i \gamma_l^i \right) \end{aligned} \quad (20)$$

$$\begin{aligned} \text{B} = & 2 \sum_{l=1}^s \sum_{g=l+1}^s \beta_l^i \beta_g^i \sum_{k=s+1}^{n+s} (t_{k-j}^i t_{k-g}^i) \\ & + \gamma_j^i \left[\sum_{k=s+1}^{n+s} (t_k^i)^2 - 2 \sum_{l=1}^s \beta_l^i \sum_{k=s+1}^{n+s} t_k^i t_{k-l}^i \right. \\ & \left. + \sum_{l=1}^s (\beta_l^i)^2 \sum_{k=s+1}^{n+s} (t_{k-l}^i)^2 \right] \end{aligned} \quad (21)$$

Combined with *Lemma 1*, the optimization problem for β_j^i is formulated as

$$\begin{aligned} \min_{\beta_j^i} f(\beta_j^i) &= (A - B)^2 \\ \text{s.t. } 1 - \sum_{j=1}^s \beta_j^i \gamma_j^i &\geq 0 \end{aligned} \quad (22)$$

To handle the inequality constraints, we further combine the Lagrange method to adjust the objective function as follows.

$$\min_{\beta_j^i} g(\beta_j^i) = \begin{cases} f(\beta_j^i), & 1 - \sum_{j=1}^s \beta_j^i \gamma_j^i \geq 0 \\ f(\beta_j^i) - \lambda \left(1 - \sum_{j=1}^s \beta_j^i \gamma_j^i\right), & \text{otherwise} \end{cases} \quad (23)$$

where λ denotes a regularization coefficient which is greater than zero. The detailed modeling procedure of GA is provided in ref. [Goldberg and Holland, 1988]. It is noted that GA is adopted as an illustrative instance to obtain the optimal parameters of PPF, and other optimization algorithms such as gradient descent and particle swarm optimization [Maclaurin et al., 2015, Bergstra and Bengio, 2012, Eggenberger et al., 2013, Lorenzo et al., 2017] can also be designed. For large-scale processes, more efficient optimization methods such as gradient descent [Maclaurin et al., 2015] is recommended.

3.2.3 Expectation Estimation Strategy

For a general first-order linear dynamic system, as proposed by Shang et al. [Shang et al., 2015], the expectations in Eq. (19) can be easily estimated with Kalman smoothing [Bishop, 2006]. Typically, the forward recursion and the backward recursion are employed to solve the problem, which, however, cannot be directly used to estimate the desired expectations for the high-order system proposed in this work.

To address this issue, we expand the dimension of the dynamic system designed in Eq. (6) as follows, and adjust it to the general form of a first-order linear dynamic system. Therefore, the general Kalman smoothing method can be easily adapted to perform the E-step.

$$\begin{aligned} \mathbf{t}_k^s &= [\mathbf{t}_k^\top, \mathbf{t}_{k-1}^\top, \dots, \mathbf{t}_{k-s+1}^\top]^\top \in \mathbb{R}^{rs}, \\ \mathbf{e}_k^s &= [\mathbf{e}_k^\top, \mathbf{0}, \dots, \mathbf{0}]^\top \in \mathbb{R}^{rs}, \\ \Phi_k &= \begin{bmatrix} \mathbf{B}_1 & \mathbf{B}_2 & \dots & \mathbf{B}_{s-1} & \mathbf{B}_s \\ \mathbf{I} & \mathbf{0} & \dots & \mathbf{0} & \mathbf{0} \\ \vdots & \vdots & \ddots & \vdots & \vdots \\ \mathbf{0} & \mathbf{0} & \dots & \mathbf{I} & \mathbf{0} \end{bmatrix} \in \mathbb{R}^{rs \times rs}, \\ \mathbf{H}_k &= [\mathbf{H}, \mathbf{0}, \dots, \mathbf{0}] \in \mathbb{R}^{m \times rs} \end{aligned} \quad (24)$$

$$\Gamma_k = \begin{bmatrix} \Gamma & \mathbf{0} & \dots & \mathbf{0} & \mathbf{0} \\ \mathbf{0} & \mathbf{0} & \dots & \mathbf{0} & \mathbf{0} \\ \vdots & \vdots & \ddots & \vdots & \vdots \\ \mathbf{0} & \mathbf{0} & \dots & \mathbf{0} & \mathbf{0} \end{bmatrix} \in \mathbb{R}^{rs \times rs} \quad (25)$$

Thereafter, the dynamic system proposed in Eq. (6) is adapted into

$$\begin{cases} \mathbf{t}_k^s = \Phi_k \mathbf{t}_{k-1}^s + \mathbf{e}_k^s \\ \mathbf{x}_k = \mathbf{H}_k \mathbf{t}_k^s + \varepsilon_k \end{cases} \quad (26)$$

where the Gaussian noise $\mathbf{e}_k^s \sim \mathcal{N}(\mathbf{0}, \Gamma_k)$.

Correspondingly, the initial conditions given by Eq. (11) become

$$\mathbf{t}_s^s = [\mathbf{t}_s^\top \ \mathbf{t}_{s-1}^\top \ \dots \ \mathbf{t}_1^\top] \sim \mathcal{N}(\mathbf{0}, \mathbf{I}_{rs}) \quad (27)$$

where $\mathbf{I}_{rs} \in \mathbb{R}^{rs \times rs}$ is an identity matrix.

After the modification, the forward recursions of Kalman smoothing [Bishop, 2006] are first applied to estimate the posterior distribution of \mathbf{t}_k^s given the total past-time \mathbf{x}_k and Θ^{old} , termed as $p(\mathbf{t}_k^s | \mathbf{x}_1, \dots, \mathbf{x}_k, \Theta^{\text{old}}) \sim \mathcal{N}(\boldsymbol{\mu}_k, \mathbf{V}_k)$, sequentially.

$$\begin{aligned}\boldsymbol{\mu}_k &= \Phi_k \boldsymbol{\mu}_{k-1} + \mathbf{K}_k (\mathbf{x}_k - \mathbf{H}_k \Phi_k \boldsymbol{\mu}_{k-1}), \\ \mathbf{P}_{k-1} &= \Phi_k \mathbf{V}_{k-1} \Phi_k^\top + \Gamma_k, \\ \mathbf{V}_k &= (\mathbf{I} - \mathbf{K}_k \mathbf{H}_k) \mathbf{P}_{k-1}, \\ \mathbf{K}_k &= \mathbf{P}_{k-1} \mathbf{H}_k^\top (\mathbf{H}_k \mathbf{P}_{k-1} \mathbf{H}_k^\top + \Sigma)^{-1}\end{aligned}\tag{28}$$

with the initialization

$$\begin{aligned}\boldsymbol{\mu}_s &= \mathbf{K}_1 \mathbf{x}_s, \\ \mathbf{V}_s &= \mathbf{I} - \mathbf{K}_1 \mathbf{H}_k, \\ \mathbf{K}_s &= \mathbf{H}_k^\top (\mathbf{H}_k \mathbf{H}_k^\top + \Sigma)^{-1}\end{aligned}\tag{29}$$

where $\boldsymbol{\mu}_k$ and \mathbf{V}_k represent the mean vector and covariance matrix of the posterior distribution, respectively. \mathbf{P}_k is the error covariance matrix of state estimate \mathbf{t}_k^s , and \mathbf{K}_k denotes the Kalman gain matrix.

Afterward, utilizing the backward recursions [Bishop, 2006] to further estimate the parameters of posterior distribution $p(\mathbf{T} | \mathbf{X}, \Theta^{\text{old}})$.

$$\begin{aligned}\hat{\boldsymbol{\mu}}_k &= \boldsymbol{\mu}_k + \mathbf{J}_k (\hat{\boldsymbol{\mu}}_{k+1} - \Phi_k \boldsymbol{\mu}_k), \\ \hat{\mathbf{V}}_k &= \mathbf{V}_k + \mathbf{J}_k (\hat{\mathbf{V}}_{k+1} - \mathbf{P}_k) \mathbf{J}_k^\top,\end{aligned}\tag{30}$$

where $\mathbf{J}_k = \mathbf{V}_k \Phi_k \mathbf{P}_k^{-1}$, and the initialization is expressed as

$$\hat{\boldsymbol{\mu}}_{n+s} = \boldsymbol{\mu}_{n+s}, \hat{\mathbf{V}}_{n+s} = \mathbf{V}_{n+s}\tag{31}$$

The derivation results between Eqs. (24) and (31), especially $\boldsymbol{\mu}_k$ and \mathbf{V}_k , are important referent variables to evaluate the expectation terms in Eq. (19).

3.3 Parameter Determination

In PPFA modeling, two parameters, the number of latent variables r and the time lag s , need to be determined before executing the EM algorithm, and the hold-out method is adopted in this work. Firstly, the normal samples are separated into two subsets with 80% as the training one and 20% as the validation one, and deviations with various magnitudes are randomly added to different observed variables in the validation subset. A relatively wide range is initialized for r and s respectively, and for each pair of r and s , the trained model is evaluated with two metrics, fault detection rate (FDR) and false alarm rate (FAR), which are defined as

$$FDR = \frac{TP}{TP + FN}\tag{32}$$

$$FDR = \frac{FP}{FP + TN}\tag{33}$$

where TP and TN are the number of correctly detected abnormal and normal samples respectively, FN is the number of faults that are not detected, and FP is the number of normal samples which are regarded as anomalies incorrectly. The (r, s) pair with the best monitoring performance in terms of FDR and FAR is chosen as the parameters of PPFA.

3.4 Monitoring Statistics Design

Once the PPFA model is established, monitoring statistical indices are of great significance when proceeding to the online monitoring part. For different indices, T^2 and SPE are the most popular ones, which assume that the data follows a Gaussian distribution [Joe Qin, 2003]. With the parameters set Θ obtained with EM and genetic algorithm, the augmented latent variable $\mathbf{t}_k^s = \Phi_k \mathbf{t}_{k-1}^s + \mathbf{K}_k (\mathbf{x}_k - \mathbf{H}_k \Phi_k \mathbf{t}_{k-1}^s)$ can be applied to define statistical indices.

$$T^2 = \mathbf{t}_k^{s\top} \mathbf{t}_k^s\tag{34}$$

$$SPE = \|\mathbf{x}_k - \mathbf{H}_k \Phi_k \mathbf{t}_{k-1}^s\|^2\tag{35}$$

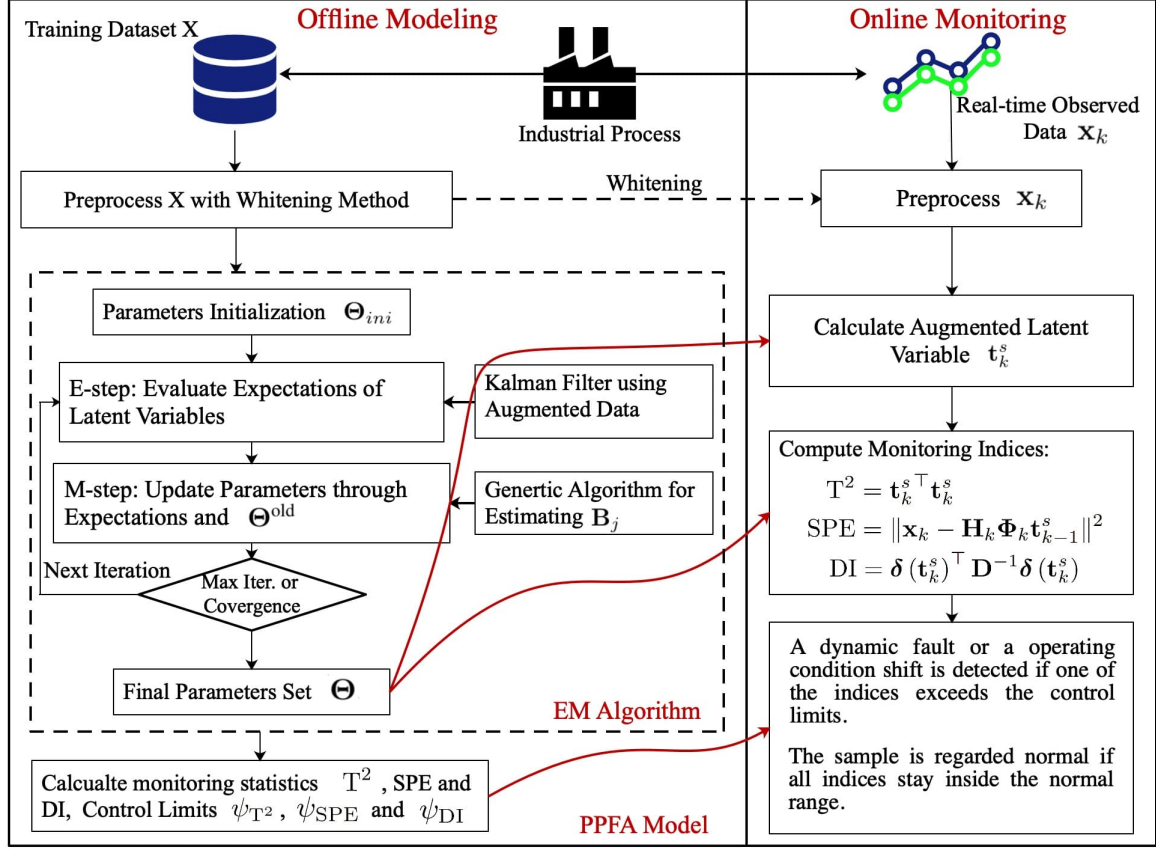


Figure 1: The schematic diagram of the proposed process monitoring method.

where the term $\mathbf{x}_k - \mathbf{H}_k \Phi_k \mathbf{t}_{k-1}^s$ represents the estimated error given the previous one-step latent variable \mathbf{t}_{k-1}^s .

Based on the established PPFA model, the derivative of latent variables which demonstrates the system dynamic changes can be easily obtained.

$$\delta(\mathbf{t}_k^s) = \mathbf{t}_k^s - \mathbf{t}_{k-1}^s \quad (36)$$

Besides, during the execution of E-step, the term $\mathbf{D} = \mathbb{E}[\delta(\mathbf{t}_k^s) \delta(\mathbf{t}_k^s)^\top]$ can be obtained as follows.

$$\mathbf{D} = \mathbb{E}[\mathbf{t}_k^s \mathbf{t}_k^{s\top}] - 2\mathbb{E}[\mathbf{t}_k^s \mathbf{t}_{k-1}^{s\top}] + \mathbb{E}[\mathbf{t}_{k-1}^s \mathbf{t}_{k-1}^{s\top}] \quad (37)$$

Motivated by the nonstationary PSFA [Scott et al., 2020], a monitoring index named Dynamic Index (DI) is developed as a supplement of T^2 and SPE to reflect the dynamics of the process.

$$\text{DI} = \delta(\mathbf{t}_k^s)^\top \mathbf{D}^{-1} \delta(\mathbf{t}_k^s) \quad (38)$$

The control limits of T^2 , SPE and DI, denoted as ψ_{T^2} , ψ_{SPE} and ψ_{DI} respectively, are determined with the kernel density estimation (KDE), which is an effective non-parametric tool [Botev et al., 2010, Martin and Morris, 1996]. Using KDE, the probability density function (pdf) of monitoring statistics is defined as

$$f(\nu) = \frac{1}{nh} \sum_{i=1}^n K\left(\frac{\nu - \nu_i}{h}\right) \quad (39)$$

where h is the bandwidth parameter, ν represents the monitoring statistics, and $K(\cdot)$ is a kernel function selected as Gaussian in this paper.

With the estimated pdf, the cumulative density function is defined as

$$P(\nu < \psi) = \int_{-\infty}^{\psi} f(\nu) d\nu \quad (40)$$

where the control limit ψ is obtained by setting a confidence level α , for example, 95%.

3.5 Proposed Monitoring Framework

The proposed PPFA based process monitoring method consists of two interrelated parts, namely offline modeling and online monitoring. Figure 1 [Ruiz-Cárcel et al., 2015] illustrates the schematic diagram of the whole monitoring framework. For the offline modeling procedure, the first step is to normalize the normal training data. In this work, the whitening procedure is applied

$$\mathbf{x}_{\text{norm}} = \mathbf{\Lambda}^{-1/2} \mathbf{U}^T \mathbf{x} \quad (41)$$

where $\mathbf{\Lambda}$ represents the singular values of the covariance matrix $\mathbf{\Omega} = \langle \mathbf{x}_k \mathbf{x}_k^T \rangle$, and \mathbf{U} is an orthogonal matrix composed of eigenvectors of $\mathbf{\Omega} \mathbf{\Omega}^T$. It is noted that the matrices $\mathbf{\Lambda}$ and \mathbf{U} are calculated by applying SVD to $\mathbf{\Omega}$, where $\mathbf{\Omega} = \mathbf{U} \mathbf{\Lambda} \mathbf{U}^T$.

After the normalization step, EM algorithm is applied to estimate the parameter set Θ . It is noted that in the E-step, as shown in Eq. (24), original data as well as parameters are augmented to simplify the Kalman smoothing process. Moreover, when executing the M-step, GA algorithm is applied to provide support for estimating \mathbf{B}_j . When the E-and-M-step loop iterates to the maximum number of iterations or convergence is acquired, the final parameter set Θ is obtained. Thereafter, according to Eqs. (34) to (40), the control limits ψ_{T^2} , ψ_{SPE} and ψ_{DI} , along with the monitoring statistics T^2 , SPE and DI can be calculated.

When it comes to the online monitoring process, the newly observed sample is first scaled with Eq. (41). Then applying the established PPFA model to calculate the augmented latent variable t_k^g conditioned on the newly measurement. Further, compute the monitoring indices T^2 , SPE and DI according to Eqs. (34) to (38). Finally, monitor if T_{new}^2 , SPE_{new} or DI_{new} exceeds its corresponding control limit.

- A dynamic process-relevant fault or a operating condition shift is detected with $(1 - \alpha) \times 100\%$ confidence level if $T_{\text{new}}^2 > \psi_{T^2}$ or $\text{DI}_{\text{new}} > \psi_{\text{DI}}$.
- If $\text{SPE}_{\text{new}} > \psi_{\text{SPE}}$, a fault that breaks the correlation of the established model is declared.
- The newly observed data is regarded as normal if $T_{\text{new}}^2 < \psi_{T^2}$, $\text{SPE}_{\text{new}} < \psi_{\text{SPE}}$ and $\text{DI}_{\text{new}} < \psi_{\text{DI}}$.

4 Experiments and Discussion

Two industrial processes, a three-phase flow facility and a medium speed coal mill, are employed in this section to illustrate the performance of the proposed monitoring scheme.

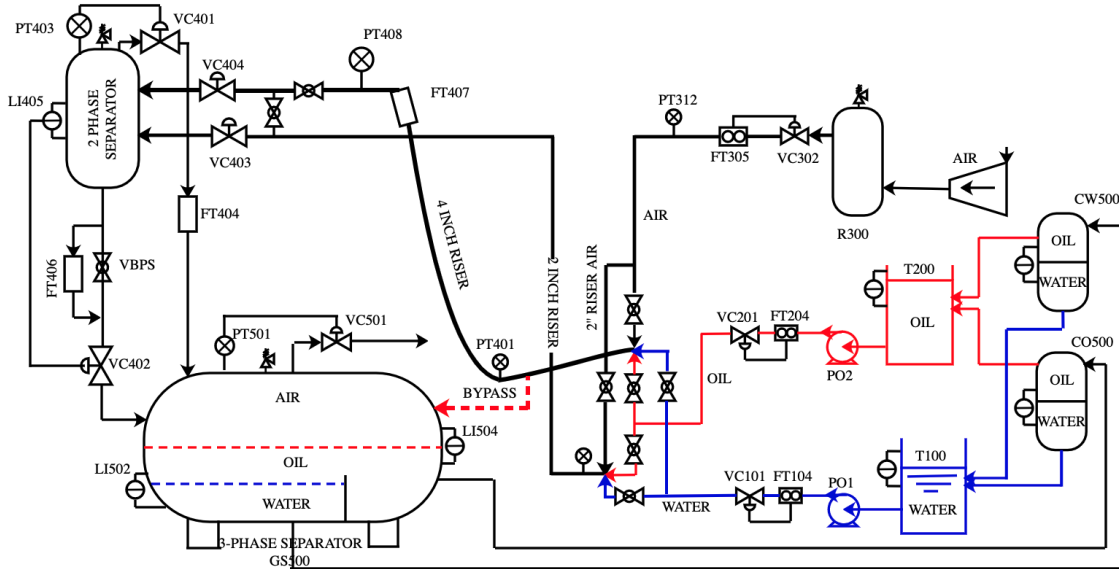


Figure 2: Sketch of three-phase flow facility.

Table 1: Set working conditions of air flow rates (m^3/s) and water flow rates (kg/s)

Air flowrate	0.0208	0.0278	0.0347	0.0417	
Water flowrate	0.5	1	2	3.5	6

Table 2: Description of data samples for modeling and monitoring

Index	Water flowrate	Air flowrate	No. samples	Description
Training data			3200	Normal
Test case 1	2	0.0417	4467	Airline blockage
Test case 2			3851	Open direct bypass

4.1 The Three-Phase Flow Facility

4.1.1 Process Description

The three-phase flow facility is a pressured system suggested by Granfield University, and it is designed for feeding a controlled and measured flow rate of water, oil and air to a pressurized system [Ruiz-Cárcel et al., 2015]. Recently, this complex system has received considerable attention and been successfully applied as a useful industrial process to evaluate the effectiveness of process monitoring methods [Zhang and Zhao, 2017, Yang et al., 2018]. As illustrated in the process diagram in Figure 2, the system is mainly composed of a two-phase separator and a three-phase separator which are connected with pipelines. It can be used to provide different products, among them are single-phase water, air and oil, or their mixtures.

A total of 24 process variables are included in the three-phase flow facility, and at a sample rate of one second, 16 sets of data are collected, the first three of which represent the normal operation status, and the remaining sets denote faulty cases of different operating conditions. For the 24 variables, the first 23 are included in all data sets, while the last is only used in fault case 6. To generate representative normal data sets, four different set points of air flow rates and five different water flow rate set points are adopted and combined into 20 different operating conditions. Set points of air flowrate and water flowrate are listed in TABLE 1. More details of this process are provided in Ref. [Ruiz-Cárcel et al., 2015].

4.1.2 Monitoring Results and Discussion

In this case study, 3200 normal samples under the combination of $0.047\text{m}^3/\text{s}$ (air flow rates) and $2\text{kg}/\text{s}$ (water flow rates) are selected as the training set. In addition, two typical fault cases, as listed in TABLE 2, are selected to verify the performance of the proposed method. To further illustrate the superiority of PPFA model, DiPCA [Dong and Qin, 2018] and PFA [Richthofer and Wiskott, 2015] are utilized to make comparisons.

Through cross validation, parameters of different models are selected: for DiPCA, the dynamic order s is set to be 3, and the number of dynamic latent variables $r = 10$. For PFA, the dimension of latent variables is 10, and the time lags is chosen as 5. In the proposed PPFA, the dynamic order s is set to be 2, and the dimension of t_k is 10. Besides, the confidence level of all methods is chosen as 99%.

Figure 3 and Figure 4 illustrate the monitoring results of test case 1 and test case 2 for different models. For test case 1, a total of 4467 measurements are collected. The fault of airline blockage is introduced continuously, and it starts from the 657th sample and ends at the 3777th sample. At the very beginning, the magnitude of fault is small, and the fault becomes more and more significant and reaches the maximum deviation between 3067th and 3777th sample. To ensure the security, the fault is removed from 3777th sample, and since then the system returns to the normal condition. From Figure 3(c), it is observed that both T^2 and SPE of PPFA start to exceed the control limit at about 1267th sample, then increase as the magnitude of the fault increases, and finally decrease after the fault is removed. For the new proposed index DI, there are three peaks, reflecting the actual significant dynamic variations in the system near the 2760th, 3067th and 3777th samples. While for DiPCA in (a) part, T^2 stays inside the normal range from the very beginning to the 2760th sample, and its SPE goes beyond its control limit from 1573th sample. It is apparent that DiPCA experiences a large delay of defecting faults compared with PPFA. In addition, though SPE of PFA in Figure 3(b) surpasses the limit since 1267th sample, T^2 tends to reach the outer space of the control limit from 2760th sample, which is also later than PPFA.

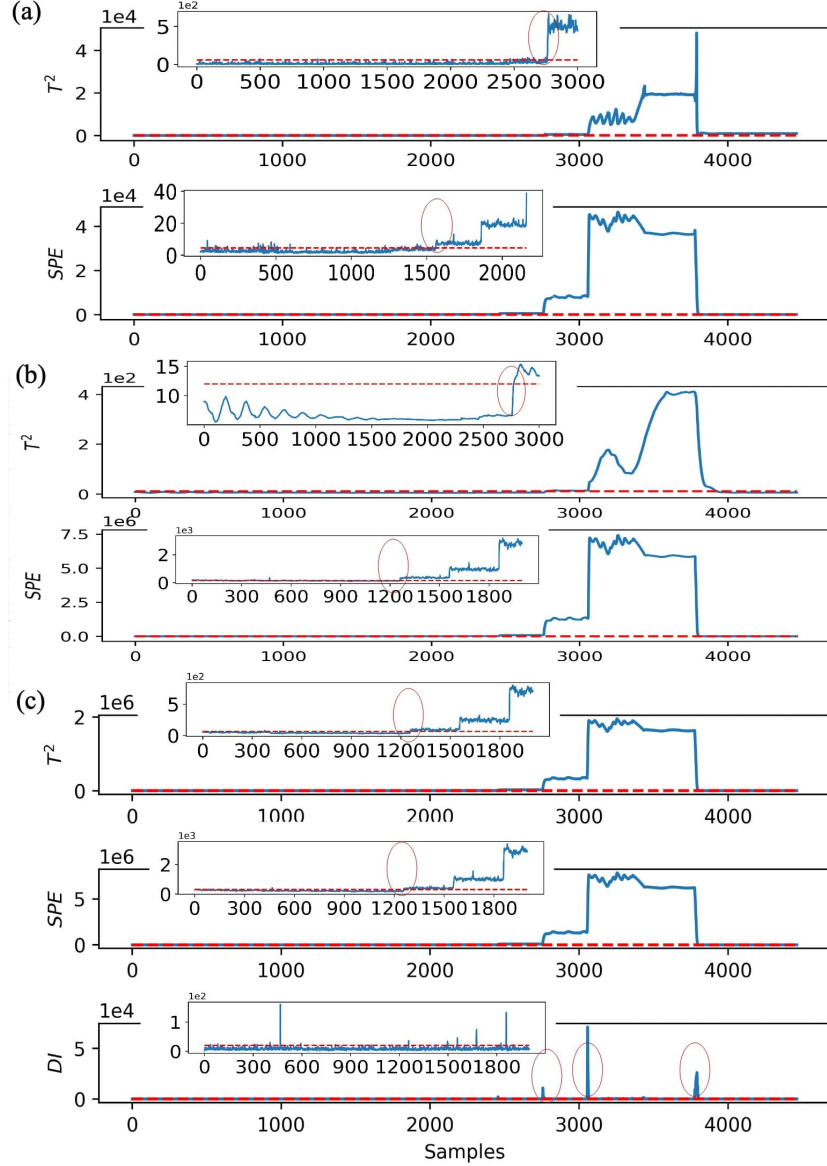


Figure 3: Monitoring results of test case 1 with (a) DiPCA, (b) PFA, and (c) PPGA.

In fault case 2, a fault of leakage is simulated by gradually opening the valve of the 4th bypass line from the 851st sample. The fault ends at 3851st and after that the process returns to a normal state. From the monitoring results in Figure 4(a), it can be seen that both T^2 and SPE of DiPCA exceed the corresponding limit from the very beginning and return to normal condition from around the 4054th sample. In Figure 4(b), T^2 is generally under the control limit and only enters the abnormal area at around the 3900th sample, leading to a poor monitoring performance. SPE stays outside of the normal region from the first sample and returns back to normal area from the 4054th sample. Obviously, both DiPCA and PFA provide limited information when monitoring fault case 2, and the model performance of PFA is worse. Figure 4(c) presents the monitoring performance of PPGA, it is observed that T^2 and SPE enter the abnormal region before the fault is introduced, which is similar to DiPCA and PFA. However, the novel designed dynamic index DI stays inside the region of normal condition before introducing the fault. It indicates that before 851s, the process is under good control, and the operating condition is different from the set point of the training set. At about the 1276th sample, DI starts to exceed the control limit, which aligns with the actual situation where the fault becomes severe. That is, the dynamic condition is disrupted from 1276s and the fault alarm of DI is worthy of attention.

Therefore, based on the above discussions, in PPFA, not only the fault but the dynamic variations of the system are involved, which shows a great superiority over DiPCA and PFA.

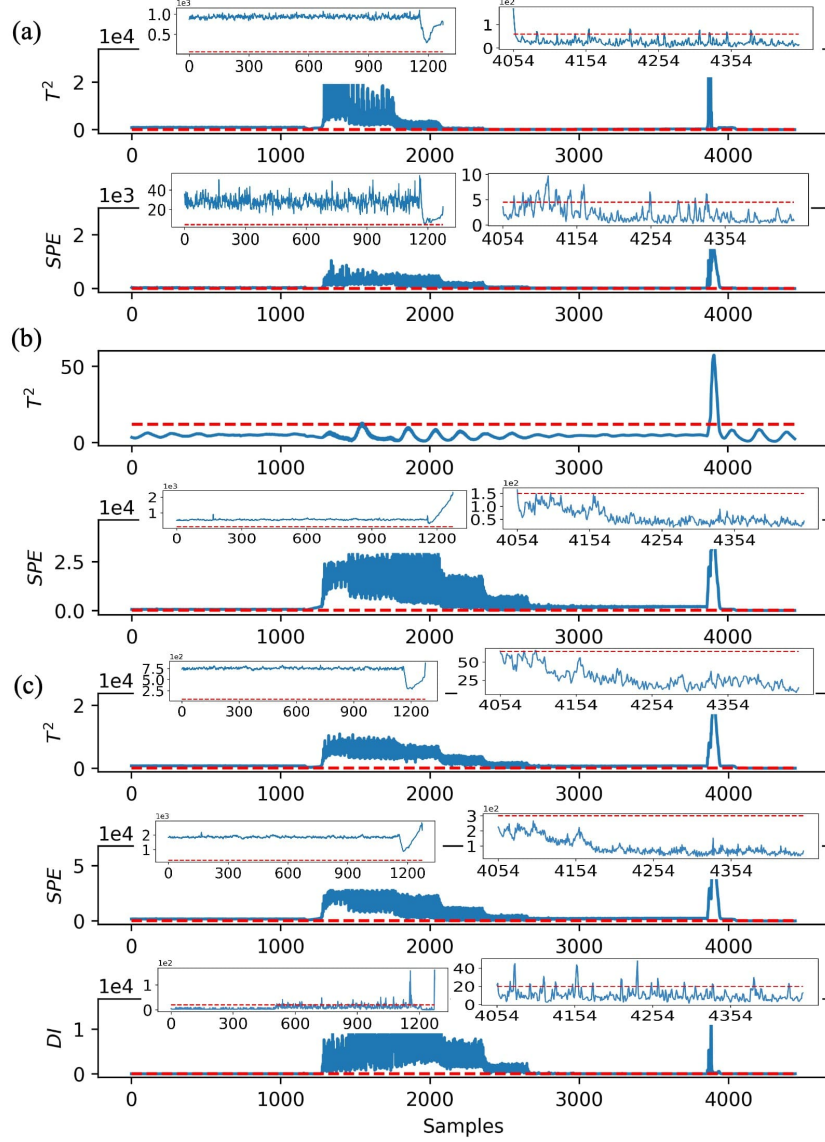


Figure 4: Monitoring results of test case 2 with (a)DiPCA, (b)PFA, and (c)PPFA.

4.2 The Medium Speed Coal Mill

4.2.1 Brief Description

To further testify the effectiveness of PPFA, two different practical fault cases happened in a ZGM-113N medium speed coal mill are employed in our work. Figure 5 depicts the schematic diagram and actual pictures of the studied coal mill. For a general medium speed coal mill, the raw materials are transported by the coal feeder into the internal space through the inlet pipe line. The raw coal falls on a grinding table rotating at a constant speed, which is further ground to coal fines. The powder that meets a certain fineness requirement is blown into the furnace by the hot primary air for combustion. The unqualified particles fall back to the coal mill under the action of gravity and inertia, and continue to be ground. As the essential auxiliary equipment, the operating status of the coal mill has an important impact on the safety and economy of the coal-fired power plant [Fan et al., 2021]. There are mainly four typical failures during the operation process, namely intrusion of foreign materials, choking, shortage of coal and fire or explosion in the mill

Table 3: Selected variables for constructing process monitoring model.

No.	Variables	Description	Unit
M1	N_{unit}	Unit load	MW
M2	M_{coal}	Coal flow rate transported by coal feeder	t/h
M3	W_{air}	Flow rate of primary air	t/h
M4	T_{air}	Temperature of primary air	$^{\circ}\text{C}$
M5	P_{air}	Pressure of primary air	kPa
M6	I_{mill}	Current of the mill's motor	A
M7	I_{feed}	Current of coal feeder's motor	A
M8	ΔP_{seal}	Difference between the pressure of seal air and primary air	kPa
M9	$T_{\text{coal-air}}$	Outlet temperature of the mixture of coal and air	$^{\circ}\text{C}$
M10	$N_{\text{coal-air}}$	Coal-air mixture outlet pressure	kPa
M11	$\Delta P_{\text{in-out}}$	Difference between the pressure of inlet and outlet of coal equipment	kPa
M12	T_{oil}	Coal mill's lubricating oil temperature	$^{\circ}\text{C}$
M13	T_{tile}	Coal mill's thrust tile temperature	$^{\circ}\text{C}$
M14	T_{bearing}	Bearing temperature of the motor	$^{\circ}\text{C}$
M15	T_{stator}	Stator winding temperature of the motor	$^{\circ}\text{C}$

[Agrawal et al., 2016]. Once a fault occurs, it is crucial to detect it as soon as possible, otherwise it may deteriorate to an irreversible damage. To sum up, discovering and maintaining different faults in time does help to ensure the safe operation of the unit and avoid economic losses.

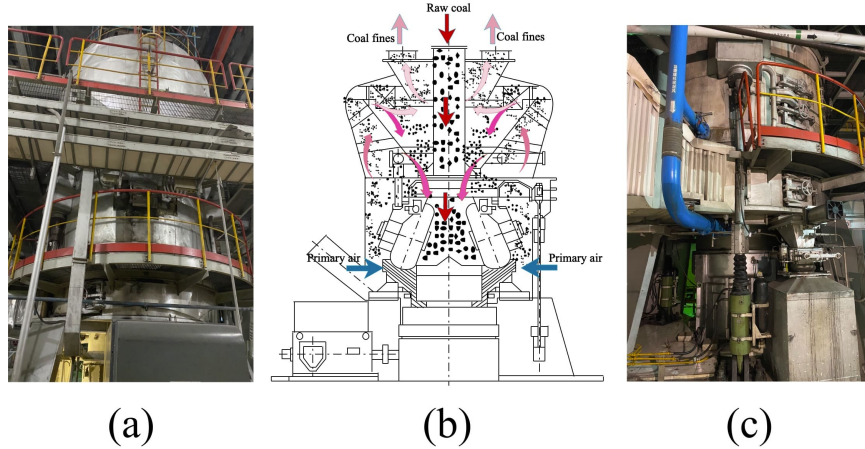


Figure 5: Schematic diagram of the medium coal mill (b)sketch, (a)(c)actual picture.

4.2.2 Monitoring Results and Discussion

In this process, two practical fault cases, mechanical failure and coal blockage, are studied. As listed in Table 3, 15 different variables are selected to build models according to the prior knowledge of coal mills [Fan et al., 2021, Cortinovis et al., 2013]. A total of normal 2385 samples are selected as the training set, and the sampling interval of the data samples is 20s. The parameters of different models are selected via cross validation: for DiPCA, $r = 10$, $s = 4$; for PFA, $r = 8$, $s = 5$; and for PPF, $r = 8$, $s = 3$. For the fault of mechanical failure, it lasts for two hours from the 94th sample to the 452th sample. Figure 6 shows the historical trends of the coal mill current and the coal flow rate. It is observed that the current fluctuates in a larger range during the fault process compared with the normal state. After maintaining the fault, some foreign matters with considerable size were found inside the mill.

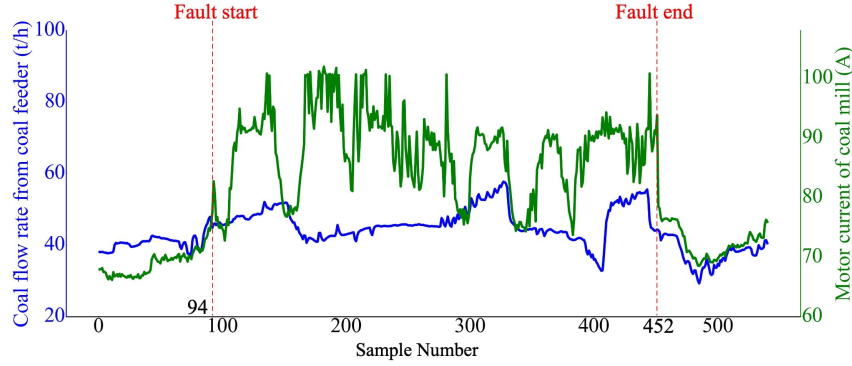


Figure 6: Historical trends of two sensors of fault case 1.

The monitoring results of DiPCA, PFA and PPFA are presented in Figure 7, in which the red dot line denotes the control limit with a 99% confidence level. For DiPCA, as reflected in Figure 7(a), both T^2 and SPE begin exceeding the control limits from around the 110th sample, and return to normal region at the 452th sample. During the process when the fault occurs, a considerable portion of the two indices stay below the control limit, leading to a relatively low fault detection rate. As observed in Figure 7(b), for PFA, the numerical value of T^2 is in an opposite trend to the actual fault, and it is lower than the red line during the occurrence of the fault, but it exceeds the threshold after the fault is removed. Though SPE follows the fault process in a good manner, the overall monitoring performance is unreliable. From the plots of PPFA's results illustrated in Figure 7(c), it can be seen that within the two hours of failure, T^2 and SPE detect the fault timely and ensure a high fault detection rate compared with DiPCA and PFA. In addition, when the coal mill current fluctuates greatly, the newly proposed index DI responds timely, and hence the dynamic characteristics of the system during the fault period are well reflected. For the second fault case, as shown in Figure 8, the coal blockage starts from the 195th sample and ends at the 435th sample. When the fault exists, the mill's current and the difference between the inlet pressure and outlet pressure have an upward trend until it is discovered and handled at about the 379th sample. During this period, the primary air flow rate continues to decrease, and starts increasing when the fault begins recovering. The coal-air mixture temperature at the export of the mill drops significantly at the beginning of the fault, and then remains at a low value until the failure ends. During the actual operation of the unit, it takes more than one hour for the fault to be discovered, which significantly delays the maintenance of the mill and causes unnecessary economic losses.

Figure 9 presents the monitoring results for the fault of coal blockage. From Figure 9(a), for the statistics T^2 and SPE it can be seen that there is a delay for near 100 samples (0.56 hour) after the disturbance happens. For the results of PFA, depicted in Figure 9(b), it shows similar pattern as it does for fault case 1. That is, though SPE retains a satisfying performance, T^2 has a poor performance which raises a large number of false alarms and obtains a low fault detection rate. For the proposed PPFA model, it is observed in Figure 9(c) that T^2 and SPE successfully raise the alarm once the fault occurs, along with a great fault detection rate. Moreover, combining with the trend of the variables in Figure 8, it can be seen that DI has obvious over-limit response to rapid fluctuations in different stages. In conclusion, considering the monitoring performance, the proposed PPFA model has great advantages over existing methods such as DiPCA and PFA. Its advantages are mainly manifested in that this method can not only realize fault detection quickly and accurately, but also the newly proposed index can be used as a supplement to reflect the dynamic changes of the system.

5 Conclusion

In this paper, a novel probabilistic predictable feature analysis method is proposed for multivariate time series monitoring. The proposed method takes measurement noise and full interpretation of dynamic characteristics into consideration. During the procedure of EM iterations, GA and Kalman filter are successfully employed to estimate parameters. In addition, a dynamic index (DI) along with T^2 and SPE is developed and applied to monitor the dynamic operation conditions of industrial processes. Through applications on the three-phase flow facility and a medium speed coal mill, the PPFA based process monitoring method has shown its effective performance compared with existing deterministic methods. Based on the monitoring results, the PPFA algorithm is worth for further investigation.

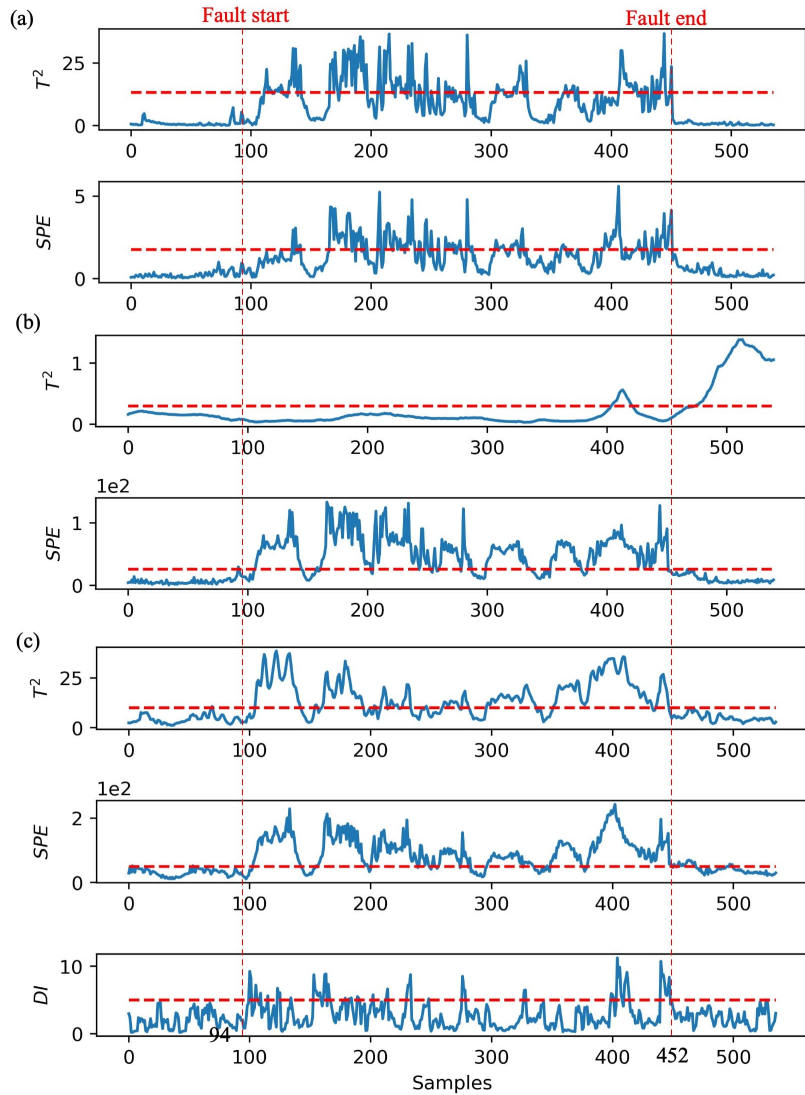


Figure 7: Monitoring results of fault case 1 with (a)DiPCA, (b)PFA, and (c)PPFA.

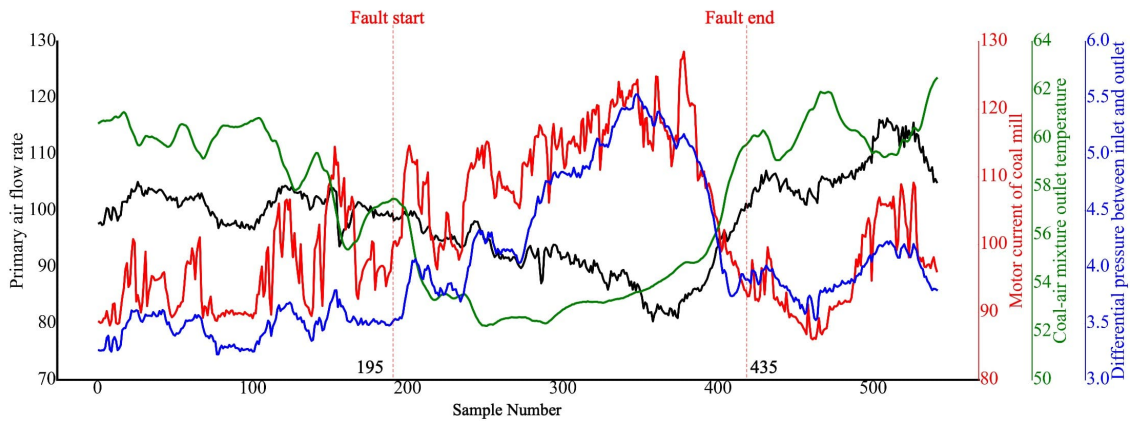


Figure 8: Historical trends of relevant sensors of fault case 2.

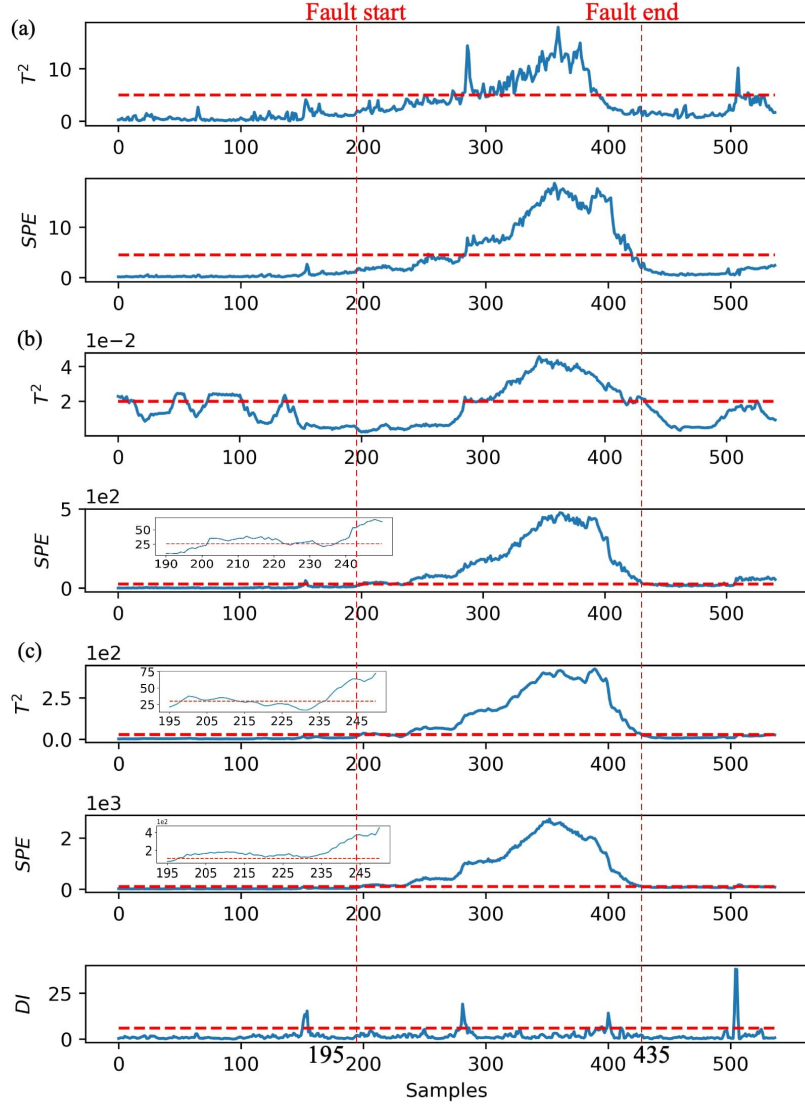


Figure 9: Monitoring results of coal blockage with (a) DiPCA, (b) PFA, and (c) PPFA.

A Proof of Lemma 1

According to Eq. (6), we have

$$t_k^i = \beta_1^i t_{k-1}^i + \cdots + \beta_s^i t_{k-s}^i + e_k^i \quad (42)$$

With the constraint $\mathbb{E}[t_k] = \mathbf{0}$, the expectation of t_k^i is

$$\mathbb{E}[t_k^i] = \beta_1^i \mathbb{E}[t_{k-1}^i] + \cdots + \beta_s^i \mathbb{E}[t_{k-s}^i] + \mathbb{E}[e_k^i] = 0 \quad (43)$$

The variance of t_k^i can be obtained with the following formula

$$\text{var}(t_k^i) = \mathbb{E}[(t_k^i)^2] - \mathbb{E}[t_k^i]^2 = \mathbb{E}[(t_k^i)^2] \quad (44)$$

Since $(t_k^i)^2 = \beta_1^{2i} t_{k-1}^i t_{k-1}^i + \cdots + \beta_s^{2i} t_{k-s}^i t_{k-s}^i + t_k^i e_k^i$, Eq. (44) is computed by

$$\mathbb{E}[(t_k^i)^2] = \beta_1^{2i} \mathbb{E}[t_{k-1}^i t_{k-1}^i] + \cdots + \beta_s^{2i} \mathbb{E}[t_{k-s}^i t_{k-s}^i] + \mathbb{E}[t_k^i e_k^i] \quad (45)$$

where the last term can be further simplified by

$$\begin{aligned}
 \mathbb{E} [t_k^i e_k^i] &= \mathbb{E} [(\beta_1^i t_{k-1}^i + \cdots + \beta_s^i t_{k-s}^i + e_k^i) e_k^i] \\
 &= \mathbb{E} [(\beta_1^i t_{k-1}^i + \cdots + \beta_s^i t_{k-s}^i) e_k^i] + \mathbb{E} [(e_k^i)^2] \\
 &= \mathbb{E} [\beta_1^i t_{k-1}^i + \cdots + \beta_s^i t_{k-s}^i] \mathbb{E} [e_k^i] + \mathbb{E} [(e_k^i)^2] \\
 &= \mathbb{E} [(e_k^i)^2] = \tau_i^2
 \end{aligned} \tag{46}$$

For ease of representation, we define

$$\begin{aligned}
 \gamma_j^i &= \text{cov} (t_k^i, t_{k-j}^i) = \text{cov} (t_{k+j}^i, t_k^i) \\
 &= \mathbb{E} [t_k^i t_{k-j}^i] - \mathbb{E} [t_k^i] \mathbb{E} [t_{k-j}^i] \\
 &= \mathbb{E} [t_k^i t_{k-j}^i]
 \end{aligned} \tag{47}$$

Therefore, the covariance in Eq. (44) simplifies to

$$\text{var} (t_k^i) = \mathbb{E} [(t_k^i)^2] = \beta_1^i \gamma_1^i + \cdots + \beta_s^i \gamma_s^i + \tau_i^2 \tag{48}$$

Since the constraint $\mathbb{E} [\mathbf{t}_k \mathbf{t}_k^\top] = \mathbf{I}_r$ has been given in Eq. (6), we have

$$\beta_1^i \gamma_1^i + \cdots + \beta_s^i \gamma_s^i + \tau_i^2 = 1 \tag{49}$$

Therefore, the relation between \mathbf{B}_j and $\mathbf{\Gamma}$ can be expressed by Eq. (7).

Acknowledgment

This work was supported by China Scholarship Council (grant numbers 202006090212), Qinglan Project of Jiangsu Province of China, National Natural Science Foundation of China under Grant 51976031 as well as the University of Waterloo. And this work has been submitted to the IEEE for possible publication. And it has been accepted by the IEEE transactions on Control Systems Technology. Copyright may be transferred without notice, after which this version may no longer be accessible.

References

- Kristen Severson, Paphonwit Chaiwatanodom, and Richard D Braatz. Perspectives on process monitoring of industrial systems. *Annual Reviews in Control*, 42:190–200, 2016.
- Zhiqiang Ge. Review on data-driven modeling and monitoring for plant-wide industrial processes. *Chemometrics and Intelligent Laboratory Systems*, 171:16–25, 2017.
- Le Zhou, Gang Li, Zhihuan Song, and S Joe Qin. Autoregressive dynamic latent variable models for process monitoring. *IEEE Transactions on Control Systems Technology*, 25(1):366–373, 2016.
- Carlos F Alcalá and S Joe Qin. Reconstruction-based contribution for process monitoring. *Automatica*, 45(7):1593–1600, 2009.
- Gang Li, S Joe Qin, and Donghua Zhou. Geometric properties of partial least squares for process monitoring. *Automatica*, 46(1):204–210, 2010.
- Qinqin Zhu, Qiang Liu, and S Joe Qin. Concurrent quality and process monitoring with canonical correlation analysis. *Journal of Process Control*, 60:95–103, 2017.
- Wenfu Ku, Robert H Storer, and Christos Georgakis. Disturbance detection and isolation by dynamic principal component analysis. *Chemometrics and intelligent laboratory systems*, 30(1):179–196, 1995.
- Tiago J Rato and Marco S Reis. Advantage of using decorrelated residuals in dynamic principal component analysis for monitoring large-scale systems. *Industrial & Engineering Chemistry Research*, 52(38):13685–13698, 2013.
- Erik Vanhatalo, Murat Kulahci, and Bjarne Bergquist. On the structure of dynamic principal component analysis used in statistical process monitoring. *Chemometrics and intelligent laboratory systems*, 167:1–11, 2017.
- Yining Dong and S Joe Qin. A novel dynamic pca algorithm for dynamic data modeling and process monitoring. *Journal of Process Control*, 67:1–11, 2018.

- Gang Li, S Joe Qin, and Donghua Zhou. A new method of dynamic latent-variable modeling for process monitoring. *IEEE Transactions on Industrial Electronics*, 61(11):6438–6445, 2014.
- Lingling Guo, Ping Wu, Siwei Lou, Jinfeng Gao, and Yichao Liu. A multi-feature extraction technique based on principal component analysis for nonlinear dynamic process monitoring. *Journal of Process Control*, 85:159–172, 2020.
- Stefan Richthofer and Laurenz Wiskott. Predictable feature analysis. In *2015 IEEE 14th International Conference on Machine Learning and Applications (ICMLA)*, pages 190–196. IEEE, 2015.
- Junhua Zheng, Zhihuan Song, and Zhiqiang Ge. Probabilistic learning of partial least squares regression model: Theory and industrial applications. *Chemometrics and Intelligent Laboratory Systems*, 158:80–90, 2016.
- Michael E Tipping and Christopher M Bishop. Probabilistic principal component analysis. *Journal of the Royal Statistical Society: Series B (Statistical Methodology)*, 61(3):611–622, 1999.
- Feihong Guo, Chao Shang, Biao Huang, Kangcheng Wang, Fan Yang, and Dexian Huang. Monitoring of operating point and process dynamics via probabilistic slow feature analysis. *Chemometrics and Intelligent Laboratory Systems*, 151:115–125, 2016.
- David Scott, Chao Shang, Biao Huang, and Dexian Huang. A holistic probabilistic framework for monitoring nonstationary dynamic industrial processes. *IEEE Transactions on Control Systems Technology*, 2020.
- Arthur P Dempster, Nan M Laird, and Donald B Rubin. Maximum likelihood from incomplete data via the em algorithm. *Journal of the Royal Statistical Society: Series B (Methodological)*, 39(1):1–22, 1977.
- Christopher M Bishop. *Pattern recognition and machine learning*. springer, 2006.
- David E Goldberg and John Henry Holland. Genetic algorithms and machine learning. 1988.
- Harish Garg. A hybrid PSO-GA algorithm for constrained optimization problems. *Applied Mathematics and Computation*, 274:292–305, 2016.
- Dougal Maclaurin, David Duvenaud, and Ryan Adams. Gradient-based hyperparameter optimization through reversible learning. In *International conference on machine learning*, pages 2113–2122. PMLR, 2015.
- James Bergstra and Yoshua Bengio. Random search for hyper-parameter optimization. *Journal of machine learning research*, 13(2), 2012.
- Katharina Eggenberger, Matthias Feurer, Frank Hutter, James Bergstra, Jasper Snoek, Holger Hoos, Kevin Leyton-Brown, et al. Towards an empirical foundation for assessing bayesian optimization of hyperparameters. In *NIPS workshop on Bayesian Optimization in Theory and Practice*, volume 10, 2013.
- Pablo Ribalta Lorenzo, Jakub Nalepa, Michal Kawulok, Luciano Sanchez Ramos, and José Ranilla Pastor. Particle swarm optimization for hyper-parameter selection in deep neural networks. In *Proceedings of the genetic and evolutionary computation conference*, pages 481–488, 2017.
- Chao Shang, Biao Huang, Fan Yang, and Dexian Huang. Probabilistic slow feature analysis-based representation learning from massive process data for soft sensor modeling. *AIChE Journal*, 61(12):4126–4139, 2015.
- S Joe Qin. Statistical process monitoring: basics and beyond. *Journal of Chemometrics: A Journal of the Chemometrics Society*, 17(8-9):480–502, 2003.
- Zdravko I Botev, Joseph F Grotowski, Dirk P Kroese, et al. Kernel density estimation via diffusion. *The annals of Statistics*, 38(5):2916–2957, 2010.
- EB Martin and AJ Morris. Non-parametric confidence bounds for process performance monitoring charts. *Journal of Process Control*, 6(6):349–358, 1996.
- Cristobal Ruiz-Cárcel, Yi Cao, D Mba, Liyun Lao, and RT Samuel. Statistical process monitoring of a multiphase flow facility. *Control Engineering Practice*, 42:74–88, 2015.
- Shumei Zhang and Chunhui Zhao. Stationarity test and bayesian monitoring strategy for fault detection in nonlinear multimode processes. *Chemometrics and Intelligent Laboratory Systems*, 168:45–61, 2017.
- Jian Yang, Zheng Lv, Hongbo Shi, and Shuai Tan. Performance monitoring method based on balanced partial least square and statistics pattern analysis. *ISA transactions*, 81:121–131, 2018.
- Wei Fan, Shaojun Ren, Qinqin Zhu, Zhijun Jia, Delong Bai, and Fengqi Si. A novel multi-mode bayesian method for the process monitoring and fault diagnosis of coal mills. *IEEE Access*, 9:22914–22926, 2021.
- Vedika Agrawal, Bijaya Ketan Panigrahi, and PMV Subbarao. Intelligent decision support system for detection and root cause analysis of faults in coal mills. *IEEE Transactions on Fuzzy Systems*, 25(4):934–944, 2016.
- Andrea Cortinovis, Mehmet Mercangoez, Tarun Mathur, Jan Poland, and Marcel Blaumann. Nonlinear coal mill modeling and its application to model predictive control. *Control Engineering Practice*, 21(3):308–320, 2013.